Article

Influence of a Meltblown Die with a Laval Airstream Channel on the Manufacturing Process of a Polymer Fiber Based on an Orthogonal Test and Simulation Analysis

Dongjun Guo and Zhisong Zhu*

Cite This: *ACS Omega* 2023, 8, 48742−48755

Read Online

ACCESS | Metrics & More | Article Recommendations

ABSTRACT: A Laval nozzle is a device that accelerates a low-speed airstream to form a high-speed airstream. In this work, we use a Laval nozzle in the airstream channel design of a meltblown die to improve the tensile properties of the fiber in the airstream field of the meltblown die. The features of the airstream field of the meltblown die are analyzed by numerical simulation. For a given parametrization, six factors may be tuned to optimize the performance of the Laval airstream channel of the meltblown die. We thus use a five-level, six-factor orthogonal test method to optimize the airstream channel of the meltblown die to determine the various factors that influence the airstream field beneath the meltblown die. The results show that the optimized Laval meltblown die performs better than the traditional die and that the widths of the larynx and expansion segment most strongly affect the airstream velocity beneath the Laval meltblown die. Compared with a traditional die, the Laval die optimized by orthogonal testing increases the peak airstream velocity by 17.54%, average velocity by 96.81%, average temperature by 12.32%, and peak pressure by 14.61% and produces weaker turbulence intensity near the spinneret. These characteristics make the airstream beneath the die more stable and uniform and accelerate the attenuation of the fiber diameter, producing more polymer nanofibers. These results demonstrate a valuable approach to the design and optimization of meltblown dies and provide a technical reference for the production and application of the meltblown fiber production equipment.
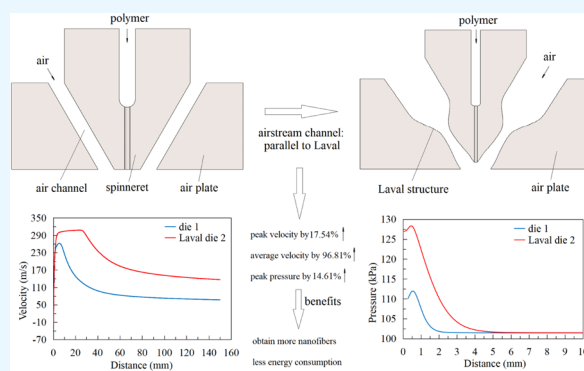
1. INTRODUCTION

Meltblown method is a nonwoven technology that uses a high-velocity and high-temperature airstream to rapidly stretch fused polymers into small-diameter fibers. Meltblown fibers have small diameters, reaching several microns or nanometers.[1−3] The meltblown process is a rapidly developing and widely used fiber-manufacturing technology, efficiently producing fibers with small diameters and large specific surface areas. Nonwoven meltblown fiber is commonly used in filter materials, heat-insulation materials, absorption materials, isolation materials, membrane materials, and so on.[4,5]

A traditional meltblown die is shown in Figure 1, the width of the air slot is 0.65 mm, the spinneret width is 2.02 mm, and the angle of the air slot is 60°, which are the sizes of a typical commercial blunt die, and most researchers use these data.[6−8] A traditional die consists of an air plate, a spinneret, a molten channel, and an airstream channel. Its working principle can be summarized as follows: the fused polymer is extruded from the spinneret hole of the meltblown die. Two high-velocity, high-temperature symmetrical airstreams rapidly stretch and refine the molten polymer, thus forming microfibers or even nanofibers, which are then collected on the net curtain to
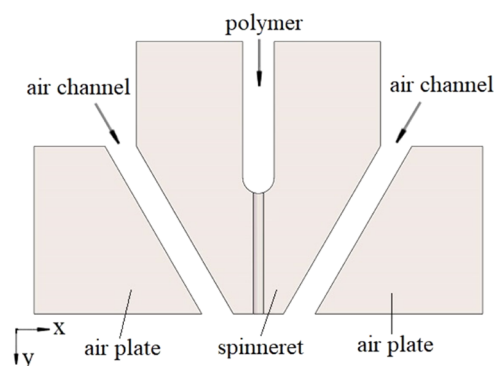
Figure 1. Structure diagram of a traditional meltblown die.
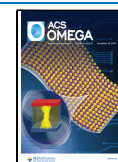
form nonwovens. The structural parameters of a meltblown die strongly affect the velocity and spread uniformity of the airstream, and the airstream field beneath the die directly determines the fiber diameter, strength, and crystallinity.[9] Significant experimental and simulation research is devoted to the structure of meltblown dies and the airstream field with the goal being to decrease the fiber diameter and obtain more nanofibers.

Harpham and Shambaugh[10,11] used a tachometer tube and a pyrometer couple to gauge the low airstream speed of a meltblown die and reported the distribution of airstream speed and temperature in the form of an empirical formula for speed and temperature in the airstream field. Bresee and Ko[12] discussed the progression of the fiber structure during melt-blowing based on experimentation. Their results indicate that the decrease in fiber diameter relies mainly on air resistance and fiber elongation around the die and airstream. Xie et al.[13,14] and Yang and Zeng[15] collected data on the airstream field and fiber motion beneath a meltblown die by using a hot wire anemometer, and the results indicate that the uniformity of the fiber diameter, the characteristics of the meltblown airstream field, and the motion of the meltblown fiber are closely linked. Yang and Zeng[16] added two types of airstream deflectors beneath a traditional meltblown die and used a two-wire probe hot wire anemometer and a high-speed camera to monitor and analyze the airstream field and fiber motion. The results show that the arrangement of the air deflector strongly affects the meltblown airstream field and fiber whipping. Hassan et al.[17] numerically and experimentally studied a new meltblown die with a vertical or inclined air contractile device and found that using a condenser makes the polymer fiber more refined. Shambaugh et al.[18] installed a pair of louvers in the airstream field beneath the meltblown die, which increases the airstream velocity on the centerline, thereby improving the economic value of the device. Zhao[19] used numerical simulation to study how the meltblown airstream field affects the fiber-stretching model, and the results show that increasing the initial airstream velocity and temperature helps to stretch and refine the fiber. Tate and Shambaugh,[20] and Harpham and Shambaugh[11] divided the meltblown double-slot airstream field into three regions: the region before the confluence of the two jets, the merging region, and the region where the two jets are merged into one. Krutka and Shambaugh[21] used computational fluid dynamics (CFD) software to simulate the airstream field and summarized the airstream field characteristics of the three regions. Krutka et al.[22,23] used CFD software to study how nozzle angle and cone angle affect the airstream under the conditions of isothermy and nonisothermy, and the results revealed that the two conditions are analogous: the hollower the head of the meltblown die, the smaller the confluence angle, the greater the mean speed on the centerline beneath the die, and the greater the amplitude of the turbulent fluctuation. Sun and Wang[24,25] combined numerical simulation and a genetic algorithm to analyze how structure factors such as airstream channel angle, airstream channel width, and die-head width affect the airstream field. The results indicate that decreasing the airstream channel angle and increasing the airstream channel width maintain the long-distance temperature, which is helpful for stretching and refinement of the fibers. Xin and Wang[8] numerically studied how the two-channel angle affects the meltblown airstream field and found that fine meltblown fiber is produced when the two-channel angle is 70°. Xie et al.[26] used CFD simulation,

particle image velocimetry, and rotation experiments to study the reflux phenomenon of the traditional meltblown fiber, and the results show that the reflux phenomenon near the spinneret hole of the die breaks the fused polymer, which degrades the fiber continuity and uniformity. Hao et al.[27] simulated the fiber movement in the meltblown process, assuming coupling between the airstream and the polymer; the results show that a higher airstream rate, a lower flow rate, and a lower polymer viscosity produce finer meltblown fibers. Yang et al.[28] compared the turbulence characteristics of two impinging jets and typical free jets to show that the characteristics of the two impinging jets provide a basis for controlling the flow field of a meltblown airstream. Han et al.[7] studied how the heat-insulated tubing affects the meltblown airstream field, and the results show that an insulated pipe increases the temperature, velocity, and turbulence of the airstream field so that a die with heat-insulated tubing produces faster fiber attenuation. Ji et al.[6] analyzed via simulation a meltblown die with an internal stabilizer and reported that the new meltblown die increases the average airstream velocity, reduces backflow, and diminishes temperature attenuation and turbulence intensity. Wang et al.[29] analyzed via simulation a new meltblown die with a cuboid bump and found that the new meltblown die produces airstream field features that help to refine the fiber. Xu et al.[30] set up a pair of nozzles under the melt-blowing mold to disrupt the secondary airstream. The results show that the fiber diameter continues to be attenuated when the velocity of the secondary airstream reaches a certain value. Hao et al.[31] studied how slot inclination affects polymer attenuation through experiments and numerical simulation and reported that the die with a slot inclination angle of 60° produces the best polymer attenuation.

Some of the investigations mentioned above improved the geometry of meltblown dies or added specific structure to the bottom of the die to produce new designs for a meltblown die, achieving some useful results. Although a few groups have focused on improving the airstream channel of the meltblown die, doing so would likely improve the meltblown airstream field and thereby lead to an ultrafine meltblown fiber. The Laval nozzle is a type of shrink-expansion nozzle invented by Gustav Patrik de Laval for steam engine applications and is now used in numerous situations.[32,33] Laval nozzles accelerate low-velocity airstreams to produce a high-velocity airstream and can even accelerate airstream from subsonic to supersonic speeds. Tan et al.[34] installed Laval nozzles under the traditional meltblown die and studied the characteristics of the meltblown airstream field with and without Laval nozzles. Laval nozzle affects the airstream field by increasing the maximum value of the fiber-stretching direction and eliminating compression waves. However, the difference is that we introduce the Laval nozzle structure into the design of the inner airstream channel of meltblown dies to improve the tensile properties of the polymer fiber in the airstream field. Instead of applying single-factor analysis to the structure of meltblown dies, as is done traditionally, we simultaneously analyze several factors that affect the Laval structure by applying a simulation analysis method. Specifically, we use a six-factor, five-level orthogonal test of the performance of a meltblown die to determine the optimal configuration. The resulting meltblown die produces an airstream field with characteristics more attractive than those of traditional meltblown dies, making it possible to produce thinner nanofibers.
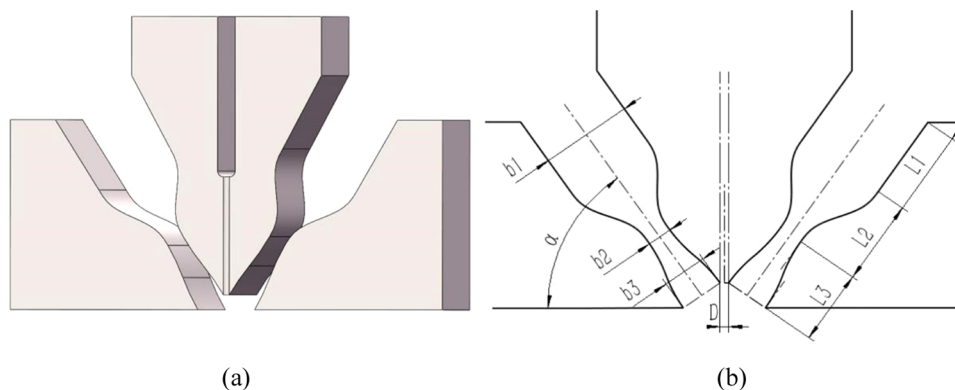
Figure 2. Structure diagram of a Laval meltblown die: (a) three-dimensional diagram of Laval meltblown die and (b) schematic diagram of Laval airstream channel.

2. MODELING AND METHOD

2.1. Turbulence Model and Governing Equation. The most used turbulence models are the two-equation turbulence model and the turbulence models containing standard $k-\varepsilon$, realizable $k-\varepsilon$, renormalization group (RNG) $k-\varepsilon$, standard $k-\omega$, and shear stress transport (SST) $k-\omega$. The SST k-ω turbulence model proposed by Menter[35] has the merits of the standard k-ε model and the $k-\omega$ model and can solve problems in domains approaching a wall and in the far field. This model adds a correction term for the reverse pressure gradient and is highly stable and accurate for analyzing flow with a high Reynolds number. The SST $k-\omega$ model is used to calculate turbulence problems and is reliable and accurate over a wide range of flow fields. It is commonly used in engineering applications.[36,37]

The fluid control equation in physics is based on three laws and is the basis of CFD simulations. The motion of polymers in the meltblown airstream field is constrained by conservation of mass. In addition, the temperature distribution in the airstream field is an important part of melt-blowing, and the exchange of thermal energy in the flow field must be considered. The basic equations of the mathematical model of the meltblown airstream field are thus the mass equation, momentum equation, energy equation, turbulent kinetic energy equation, and specific dissipation rate equation.[35,38,39]

We need not consider the dynamic flow field to simulate a steady-state incompressible two-dimensional (2D) flow field. The mass equation thus takes the form

$$\frac{\partial u}{\partial x} + \frac{\partial v}{\partial y} = 0 \tag{1}$$

where u and v are the x and y components of the airstream velocity.

All flow problems must obey conservation of momentum, which is Newton's second law

$$\frac{\partial(\rho u)}{\partial t} + \text{div}(\rho u \overline{v}) = -\frac{\partial P}{\partial x} + \frac{\partial \tau_{xx}}{\partial x} + \frac{\partial \tau_{yx}}{\partial y} + F_x$$

$$\frac{\partial(\rho v)}{\partial t} + \text{div}(\rho v \overline{v}) = -\frac{\partial P}{\partial y} + \frac{\partial \tau_{xx}}{\partial x} + \frac{\partial \tau_{yx}}{\partial y} + F_y \tag{2}$$

where P is the pressure on the airstream microelement, ρ is airstream density, τ_{xx} and τ_{xy} are the components of viscosity stress acting on the microcell face, and F_x and F_y are the volume forces on the microelement.

In the airstream with heat exchange, the conservation of energy must be obeyed. The energy of the fluid is usually composed of internal energy, kinetic energy, and potential energy. The equation for conservation of energy as a function of air temperature T is

$$\frac{\partial(\rho T)}{\partial t} + \text{div}(\rho \overline{u} T) = \text{div}\left(\frac{k_a}{c_p}\text{grad } T\right) + S_T \tag{3}$$

where c_p is the specific heat at constant pressure, k_a is the heat exchange coefficient of the airstream, and S_T is the source term and the part where viscous action is converted into thermal energy.

The equation of turbulent kinetic energy k is

$$\frac{\partial(\rho k)}{\partial t} + \frac{\partial(\rho k u_i)}{\partial x_i} = \frac{\partial}{\partial x_j}\left(\Gamma_k \frac{\partial k}{\partial x_j}\right) - Y_k + G_k + S_k \tag{4}$$

where μ_i is the velocity component, Γ_k is the effective diffusion coefficient of k, S_k is the source term of k, G_k is the generating term of k, and Y_k is the dissipation of k.

The equation for the specific dissipation rate ω is

$$\frac{\partial(\rho \omega)}{\partial t} + \frac{\partial(\rho \omega u_i)}{\partial x_i} = \frac{\partial}{\partial x_j}\left(\Gamma_\omega \frac{\partial k}{\partial x_j}\right) - Y_\omega + G_\omega + D_\omega + S_\omega \tag{5}$$

where Γ_ω is the effective diffusion coefficient of ω, S_ω is the source term of ω, Y_ω is the dissipative term of ω, D_ω is the cross-dissipative term of ω, and G_ω is the generating term of ω.

2.2. Modeling Laval Meltblown Die. To obtain a greater airstream velocity on a spinning centerline below the spinneret hole and improve the refinement of the meltblown fiber, as shown in Figure 2a, we designed a meltblown die incorporating a Laval nozzle structure. The parallel airstream channel of a traditional die is changed to a Laval nozzle structure in the proposed die, and a Laval airstream channel structure appears on each side of the proposed meltblown die. The Laval airstream channel is an axisymmetric structure composed essentially of four parts: a stable segment, a contraction segment, a larynx segment, and an expansion segment. The stable segment is composed of two parallel segments that reduce the deflection angle of the airstream, reduce the turbulence of the airstream into the contraction segment, and stabilize the airstream. The contraction segment serves to accelerate the airstream and, at the same time, ensure that the

outlet airstream of the contraction segment is uniform and stable. The contraction segment is composed of a quintic curve, as described by Formula 6. The contraction of the final segment of the quintic curve is relatively gentle, the inlet criterion is improved, the outlet airstream is more uniform, and the larynx is shorter. The expansion segment is composed of arcs and continues to accelerate the airstream, accelerating the sonic flow in the larynx to supersonic velocity. Figure 2b shows the following structural parameters of the Laval airstream channel: b_1 is the entrance width of the contraction segment, b_2 is the larynx width, b_3 is the outlet width of the expansion segment, L_1 is the length of the stable segment, L_2 is the length of the contraction segment, L_3 is the length of the expansion segment, α is the inclination of the airstream channel, and D is the diameter of the spinneret hole. The equation for the contraction segment is

$$b = (b_1 - b_2)\left[1 + \frac{b_2}{b_1 - b_2} - 10\left(\frac{x}{L_2}\right)^3 + 15\left(\frac{x}{L_2}\right)^4 - 6\left(\frac{x}{L_2}\right)^5\right] \tag{6}$$

2.3. Meshing and Boundary Conditions. The airstream field inside and outside the meltblown die has a characteristic two-dimensional distribution, so the structure of the meltblown die can be simplified to a two-dimensional axisymmetric model. The calculation region of the meltblown airstream field thus shrinks to half of the total airstream field. The two-dimensional airstream field can obtain more accurate and reliable computing results, which saves computing time and resources.[18] Figure 3 shows the calculation region of the airstream field of the Laval meltblown die. Point O is the origin of the coordinate system and is in the center of the outlet hole. The line segment OP is the spinning centerline, the y axis is in the direction of the velocity of the spinning fiber, and the x-axis
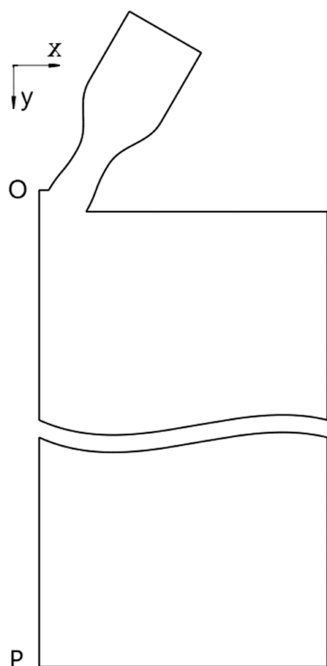
Figure 3. Calculation domain.

direction is perpendicular to the y axis. The calculation region of the airstream field beneath the die is a regular rectangle 150 mm long and 25 mm wide. The boundary of the airstream channel of the meltblown die is irregular, reflecting a more complex airstream state. In addition, the airstream field beneath the die is a significant area for analyzing the performance of the meltblown die, so the mesh for the whole area, including the airstream channel and the area below the die, must be encrypted. Figure 4 shows the mesh
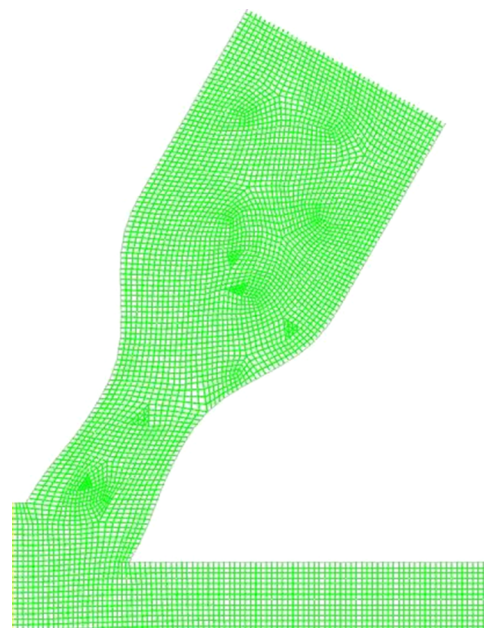
Figure 4. Grid magnification of the local area of airstream channel after encryption.

(magnified in some areas of the airstream channel) after grid encryption. The same meshing method is used for all models studied herein, and the number of mesh elements falls between 370,000 and 385,000.

The simulation considers hot air as the fluid and furthermore assumes air to be an ideal gas. The results should therefore be similar to those of the real gas model. The airstream inlet is defined as a pressure inlet, the airstream outlet is defined as a pressure outlet, and a nonslip and nonseepage wall boundary is assumed. Table 1 lists the calculation parameters.

Table 1. Value of Boundary Condition

name	pressure (atm)	temperature (K)
pressure inlet	1.4	543
pressure outlet	1	300
wall		543

3. RESULTS AND DISCUSSION

3.1. Single-Factor Analysis of the Performance of the Meltblown Die. Table 2 shows the initial parameters of a meltblown die with two Laval airstream channels. The meltblown die made with the initial data is recorded as Laval die 1. The Laval nozzle structure and the meltblown die structure are such that the parameters of the former are constrained to vary within a certain range, which necessarily

Table 2. Original Value of Laval Die

	b_2 (mm)	b_1/b_2	b_3/b_2	L_2/b_2	L_3/b_2	L_1/b_1
original value	1.0	2.4	1.25	2.1	1.0	1.6

varies the performance of the meltblown die. We now apply a single-factor analysis to discuss, based on the simulation with given boundary conditions, how the six parameters of the Laval nozzle affect the spinning characteristics of the meltblown die. The six factors are the larynx width b_2 and five dimensionless factors b_1/b_2, b_3/b_2, L_2/b_2, L_3/b_2, and L_1/b_1. The single-factor analysis allows us to determine the optimal size of the Laval airstream channel for the meltblown die in order to select the level values of the factors in the following orthogonal test.

3.1.1. Effect of b_2 on the Performance of the Meltblown Die. The larynx width of the Laval nozzle strongly influences its performance. For the meltblown die, the minimum width of the airstream channel affects the airstream speed and temperature along the spinning centerline beneath the spinneret hole and also determines the energy consumption of the meltblown process. If the minimum width (larynx width) of the airstream channel of the Laval meltblown die is too small, the effective length of the airstream stretch on the spinning centerline below the spinneret is too short to adequately refine the fiber. If the larynx width is too large, then the energy consumption is excessive, which increases production costs. Therefore, the larynx width of the airstream channel should be intermediate. With the other structural parameters held constant, the larynx width b_2 is assigned eight values: 0.6, 1.0, 1.4, 1.8, 2.2, 2.6, 3.0, and 3.4 mm. Figure 5 shows the resulting distribution of the maximum velocity (peak velocity) along the spinning line beneath the meltblown die as a function of the larynx width.
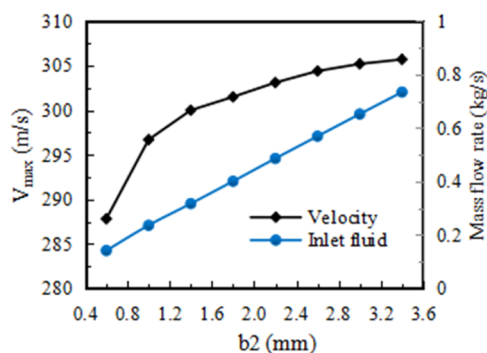
Figure 5. Maximum airstream velocity and mass flow rate as functions of the larynx width.

The results in Figure 5 indicate that the maximum velocity along the spinning line beneath the meltblown die increases with increasing larynx width. When the larynx width is less than 1.4 mm, the maximum velocity increases at a high rate with respect to the larynx width and then increases more gently when the larynx width is greater than 1.4 mm. However, the larger the larynx width, the more the gas and energy are consumed in the fiber production process. As shown in Figure 5, when the larynx width increases by 0.4 mm, the increment of the mass flow rate of the meltblown die is basically the same, about 0.09 kg/s, while the increment of the maximum airstream velocity of the meltblown die decreases gradually. As can be seen from the curve in the figure, when the larynx

width increases from 0.6 to 3.4 mm, the increase of the maximum airstream velocity of the meltblown die is 8.966, 2.758, 1.956, 1.844, 1.429, 0.642, and 0.282 mm, respectively. Therefore. it is uneconomical to sacrifice greater energy consumption to achieve a lower growth rate, which undoubtedly increases the cost of production and is an unwise choice.

3.1.2. Effect of b_1/b_2 on the Performance of the Meltblown Die. At the onset of contraction of the Laval airstream channel, the airstream velocity is relatively low. The airstream can be accelerated (even to the sound velocity) by reducing the width of the contraction segment. In addition to the shape of the contraction segment, the entrance width of the contraction segment also affects the performance of the Laval structure. The ratio b_1/b_2 of the entrance width to the larynx width of the contraction segment affects the acceleration of the airstream in the contraction segment. With the other parameters held constant, seven ratios b_1/b_2 (1.2, 1.6, 2.0, 2.4, 2.8, 3.2, and 3.6) are tested to determine the distribution of the peak airstream velocity along the spinning line beneath the meltblown die. Figure 6 shows the maximum airstream velocity as a function of the ratio b_1/b_2.
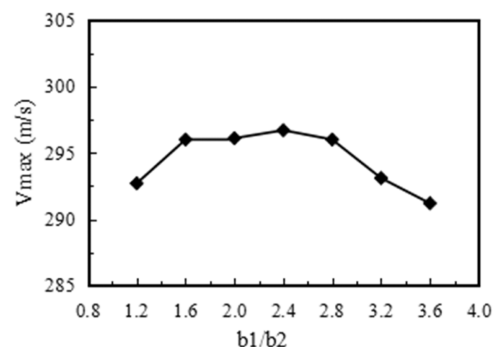
Figure 6. Maximum airstream velocity as a function of the ratio b_1/b_2.

The results in Figure 6 show that the peak airstream velocity along the spinning line beneath the meltblown die goes through a maximum at $b_1/b_2 = 2.4$ as b_1/b_2 increases. For a single Laval nozzle, as b_1/b_2 increases to 2.4, the contraction angle increases, the airstream enters the contraction channel under a higher inlet pressure, the air pressure decreases gradually, and the airstream velocity increases gradually. After the confluence of the two airstreams, the airstream velocity also increases gradually. As b_1/b_2 exceeds 2.4, the curve of the contraction segment of the single Laval nozzle becomes steeper, the resistance of the airstream increases, and the pressure difference at the entrance and outlet of the contraction segment decreases, which seriously reduces the acceleration of the airstream in the contraction segment and the maximum airstream velocity on the spinning line decreases gradually when the airstream of the two channels converges. Therefore, with the other parameters held constant, the "knee" of the maximum air velocity curve is the best choice, i.e., $b_1/b_2 = 2.4$.

3.1.3. Effect of b_3/b_2 on the Performance of the Meltblown Die. According to the structure and principle of the Laval nozzle, the airstream velocity increases upon approaching the larynx region, even to the sound velocity, and the expansion segment behind the larynx continues to accelerate the airstream. The ratio of b_3/b_2 of the outlet width

of the expansion segment to the larynx width determines the Mach number that can be achieved. With the other parameters held constant, the ratio b_3/b_2 reflects the expansion angle of the expansion segment, which determines the acceleration of the airstream in the expansion segment. Seven values (1.05, 1.15, 1.25, 1.35, 1.45, 1.55, and 1.65) for the ratio b_3/b_2 were tested to determine the peak airstream velocity along the spinning line beneath the meltblown die. Figure 7 shows the maximum airstream velocity as a function of b_3/b_2.
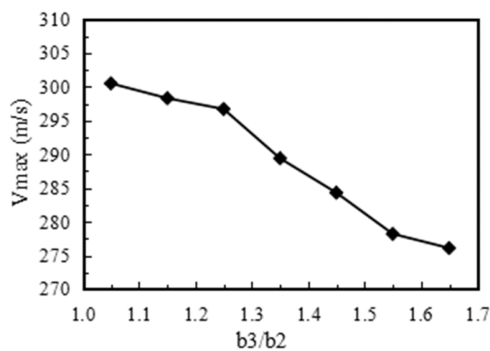
Figure 7. Maximum airstream velocity as a function of the ratio b_3/b_2.

The results in Figure 7 show that the airstream peak velocity along the spinning line below the meltblown die decreases gradually as b_3/b_2 increases. According to the principle of the Laval nozzle, an excessively large expansion angle creates serious shock waves at the outlet of the nozzle, which leads to rapid diffusion of the airstream. Conversely, an excessively small expansion angle creates boundary layer thickness and pressure loss, which decreases the airstream velocity. The transition from the larynx to the dilated segment should be smooth, so a large value of b_3/b_2 is not suitable; this ratio should be as small as possible. If $b_3/b_2 = 1$, the expansion segment has a constant width and becomes a parallel larynx of a certain length, and the airstream is not accelerated. Therefore, when the other structural parameters are held constant, the optimal value of b_3/b_2 is 1.05.

3.1.4. Effect of L_2/b_2 on the Performance of the Meltblown Die. The function of the contraction segment of the Laval structure is to accelerate the airstream with the outlet airstream being uniform, straight, and stable. In addition, the front part should not be separated and the rear flow field should be uniform. In addition to the profile type and entrance width of the shrinking segment, the length L_2 of the shrinking segment also affects the performance of the Laval nozzle. The ratio of L_2/b_2 of the length of the contraction segment to the width of the larynx reflects the acceleration and stability of the airstream in the contraction segment. With the other parameters held constant, seven values were selected for L_2/b_2 (0.9, 1.2, 1.5, 1.8, 2.1, 2.4, and 2.7) to determine the peak velocity of the airstream on the spinning line beneath the meltblown die. Figure 8 shows the airstream peak velocity as a function of L_2/b_2.

The results in Figure 8 indicate that the peak airstream velocity along the spinning line under the meltblown die increases continuously as L_2/b_2 increases from 0.9 to 1.2 and then decreases as L_2/b_2 increases from 1.2 to 1.5. When L_2/b_2 = 1.5−2.1, the maximum airstream velocity increases monotonically because the pressure difference between the inlet and the larynx of the contraction segment increases as $L_2/$
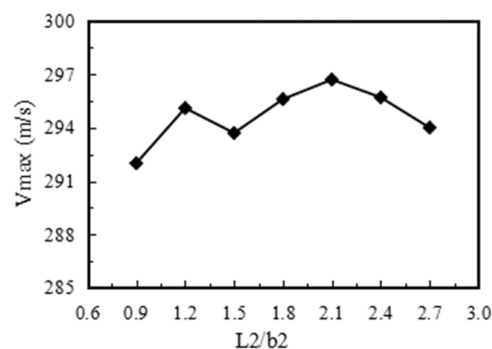
Figure 8. Maximum airstream velocity as a function of the ratio L_2/b_2.

b_2 increases, which makes the airstream more stable and accelerate continuously. When L_2/b_2 = 2.1, the airstream peak velocity is maximal. When L_2/b_2 > 2.4, the airstream peak velocity decreases gradually because the airstream accelerates over a longer distance, which can make the airstream more uniform and stable, but at the same time, it also increases the attenuation of airstream kinetic energy, so the maximum airstream velocity becomes smaller. Considering the cost of the equipment, the shrinkage segment should not be too long. However, to ensure a uniform airstream, the shrinkage segment should not be too short. Therefore, to ensure the airstream acceleration feature of the contraction segment, L_2/b_2 = 2.1, with the other structural parameters unchanged.

3.1.5. Effect of L_3/b_2 on the Performance of the Meltblown Die. The expansion segment can further accelerate the sonic flow of the larynx to supersonic. In addition to the profile shape and outlet width of the expansion segment, the length L_3 of the expansion segment also has a certain influence on the performance of the Laval nozzle. The ratio of L_3/b_2 of the length of the expansion segment to the width of the larynx determines the acceleration capacity of the airstream in the expansion segment. With the other parameters held constant, seven values for L_3/b_2 (0.4, 0.6, 0.8, 1.0, 1.2, 1.4, and 1.6) were selected to determine the distribution of the peak airstream velocity along the spinning line beneath the meltblown die. Figure 9 shows the maximum airstream velocity as a function of L_3/b_2.
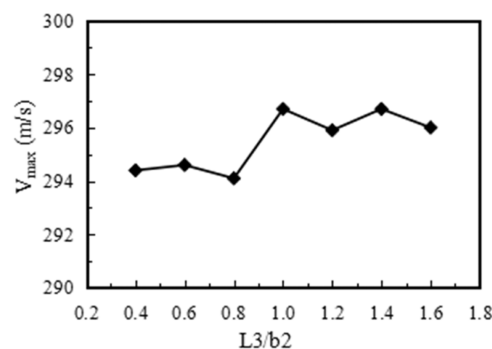
Figure 9. Maximum airstream velocity as a function of the ratio L_3/b_2.

The results in Figure 9 show that, upon increasing L_3/b_2, the airstream peak velocity on the spinning line beneath the meltblown die varies irregularly in a wavy manner. According to the principle of the Laval nozzle, the airstream produces shock waves in the expansion segment, and the airstreams on both sides of the meltblown die converge beneath the

spinneret hole. The velocity of the convergent airstream depends on the length of the expansion segment, so the airstream velocity varies as a function of the length of the expansion segment. However, overall, the maximum airstream velocity essentially increases initially and then decreases with increasing L_3/b_2. When $L_3/b_2 = 1.0$, the velocity of the airstream is maximal. Therefore, with the other structural parameters held constant, the optimal configuration is $L_3/b_2 = 1.0$.

3.1.6. Effect of L_1/b_1 on the Performance of the Meltblown Die. The stable segment reduces the airstream deflection angle, guides the uniform airstream into the Laval structure, and diminishes the turbulence, thereby helping stabilize the airstream. In addition to the width of the stable segment, the length L_1 of the stable segment also affects the airstream velocity and stability in the Laval nozzle. The ratio L_1/b_1 of length to width of the contraction segment reflects the stability of the airstream in the contraction segment. With the same other parameters held constant, eight values of L_1/b_1 are selected (0.4, 0.7, 1.0, 1.3, 1.6, 1.9, 2.2, and 2.5) to determine the distribution of the peak airstream velocity along the spinning line beneath the meltblown die. Figure 10 shows the maximum airstream velocity as a function of L_1/b_1.
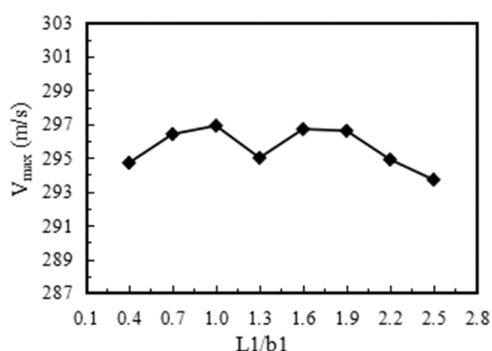
Figure 10. Maximum airstream velocity as a function of the ratio L_1/b_1.

The results in Figure 10 show that as L_1/b_1 increases to 1.0, the airstream peak velocity along the spinning line beneath the meltblown die increases gradually. As L_1/b_1 increases from 1.0 to 1.6, the maximum airstream velocity decreases initially and then increases, and when $L_1/b_1 > 1.6$, the maximum airstream velocity decreases gradually. Overall, the maximum air velocity essentially increases initially and then decreases. When $L_1/b_1 = 1.0$, the airstream velocity is maximal. An increase in L_1/b_1 equates to an increase in the length L_1 of the stable segment. This increases the stability of the airstream, allowing it to convert more internal energy into kinetic energy, thereby further accelerating the airstream. However, if the stable segment is too long, the airstream flows longer in the stable segment, increasing the internal friction between the fluid and the wall and within the fluid itself, resulting in the loss of fluid kinetic energy. In addition, a longer stable segment increases the production cost. Thus, an excessively long stable segment results in a smaller peak airstream velocity. However, shortening the stable segment destabilizes the fluid, which degrades the stretching of the fiber beneath the meltblown die. Therefore, if the other structural parameters remain unchanged, then we select $L_1/b_1 = 1.0$ to maximize the airstream peak velocity.

3.1.7. Results of Single-Factor Optimization. Under the condition that other parameters and analysis methods are unchanged, the influence of only one structural parameter on the performance of the Laval meltblown die is analyzed, and the above six optimal single-factor results are obtained. The single-factor analysis provides a basis for the selection of the level values of the factors in the following orthogonal test.

3.2. Multifactor Analysis of Meltblown Die Performance by an Orthogonal Test. The preceding analysis gives the parameter values for an optimal Laval airstream channel in conjunction with the meltblown die. Unfortunately, when varying single factors, all of the other structural parameters were held constant. If the parameters have other values, optimization of the meltblown die is no longer guaranteed. Therefore, multifactor analysis of the meltblown die is required to ensure an optimal combination of structural parameters.

3.2.1. Design of the Orthogonal Test. In practical applications, orthogonal tests are often used to analyze problems with multiple factors and multiple levels. The orthogonal test offers the significant advantage of selecting more factors and levels as test points, thereby requiring fewer tests and less manpower, material, and financial resources; therefore, it is a fast and economical test method. Therefore, we use the orthogonal test analysis to analyze the six parameters that affect the performance of the Laval meltblown die.

The design of the orthogonal experiment is based mainly on the comprehensive test scheme defined by the experimental design table. For an orthogonal test, an orthogonal table is usually created to analyze the test results, which take the form $L_n(t^c)$, where L identifies the orthogonal table, n is the number of tests, t is the number of levels, and c is the number of factors. By using the simulation, an orthogonal test was done using the six factors b_2, b_1/b_2, b_3/b_2, L_2/b_2, L_3/b_2, and L_1/b_1 for the Laval meltblown die. To satisfy the requirements of the orthogonal table, each of the six factors takes five horizontal values, as shown in Table 3. Therefore, as mentioned above, a total of 25

Table 3. Orthogonal Level List

	factors					
	A	*B*	*C*	*D*	*E*	*F*
levels	b_2 (mm)	b_1/b_2	b_3/b_2	L_2/b_2	L_3/b_2	L_1/b_1
1	1	2	1.05	1.9	0.4	0.5
2	1.2	2.3	1.1	2.1	0.6	0.7
3	1.5	2.6	1.15	2.3	0.8	0.9
4	1.8	2.9	1.2	2.5	1	1.1
5	2	3.2	1.25	2.7	1.2	1.3

tests are required and are recorded as $L_{25}(5^6)$. The orthogonal table is presented in Table 4. The other conditions remain unchanged to ensure that the performance of the meltblown die is optimal. We input each group of data from the orthogonal test table into the simulation, carry out the numerical simulation of different configurations, and input the simulation results into the last column of the orthogonal test table (Table 4).

3.2.2. Range Analysis. Range analysis is an important analysis method in the orthogonal test method and can directly determine how factors and levels affect the measurement results. Range analysis is a method to calculate the range of the data obtained by numerical simulation, producing the optimal

Table 4. Orthogonal List and Test Results of L_{25} (5^6)

	A	B	C	D	E	F	V_{max} (m/s)
1	1	1	1	1	1	1	303.303
2	1	2	2	2	2	2	302.017
3	1	3	3	3	3	3	300.195
4	1	4	4	4	4	4	298.243
5	1	5	5	5	5	5	297.45
6	2	1	2	3	4	5	301.31
7	2	2	3	4	5	1	303.121
8	2	3	4	5	1	2	300.882
9	2	4	5	1	2	3	298.127
10	2	5	1	2	3	4	302.88
11	3	1	3	5	2	4	302.903
12	3	2	4	1	3	5	303.891
13	3	3	5	2	4	1	301.536
14	3	4	1	3	5	2	304.89
15	3	5	2	4	1	3	304.382
16	4	1	4	2	5	3	304.649
17	4	2	5	3	1	4	302.979
18	4	3	1	4	2	5	305.976
19	4	4	2	5	3	1	305.206
20	4	5	3	1	4	2	304.244
21	5	1	5	4	3	2	303.856
22	5	2	1	5	4	3	305.395
23	5	3	2	1	5	4	305.262
24	5	4	3	2	1	5	304.575
25	5	5	4	3	2	1	303.534

configuration. First, the mean value k_i of level i is calculated for each factor, as shown in Formula 7

$$k_i = \frac{1}{t} K_i = \frac{1}{t} \sum_{j=1}^{t} y_{ij} \tag{7}$$

where j is the order of factors, K_i is the sum of the results for level i, y_{ij} is the factor j and the level result i, and k_{ij} is the average value of the sum of the j factor and the i level results. The range R_j is then calculated by using Formula 8

$$R_j = \max(k_{1j}, k_{2j}, k_{3j}, ..., k_{ij}) - \min(k_{1j}, k_{2j}, k_{3j}, ..., k_{ij}) \tag{8}$$

The range is the difference between the average maximum and the average minimum at level j.

The higher the value of R_j, the more sensitive the measurement is to the factor. In other words, the more susceptible the factor is to the measurement results; thus, the significance of the test level can be measured intuitively from the measurement results. Table 5 gives the results of the range analysis for the orthogonal test. Ranking the factors in terms of how strongly they affect the maximum airstream velocity of the meltblown die gives the following results: A (larynx width) > C (the ratio b_3/b_2 of the outlet width of the expansion segment to the larynx width) > B (the ratio b_1/b_2 of the entrance width to the larynx width of the contraction segment) > E (the ratio L_3/b_2 of the length of the expansion segment to the width of the larynx) > F (the ratio L_1/b_1 of length to width of the contraction segment) > D (the ratio L_2/b_2 of the length of the contraction segment to the width of the larynx). The ranges for b_2 and b_3/b_2 are much greater than those of other factors, so b_2 and b_3/b_2 are significant factors. In practical production and application, priority should be given to the ratio of the outlet width to the larynx width, and the influence of any factor on the performance of meltblown dies is analyzed by multifactor analysis.

As shown in Table 5, the parametrization that produces the maximum airstream velocity of a meltblown die is A4B2C1D1E1F1. A new meltblown die was thus designed based on the optimal factors and named "Laval die 2." However, as mentioned earlier, shortening the length of the stable segment destabilizes the fluid, which disturbs the fiber. Given that the fibers cohere easily, this would be disadvantageous to fiber-stretching beneath the meltblown die. Because L_1/b_1 is a nonsignificant factor and has little effect on the features of the meltblown die, the stable segment can be lengthened appropriately to improve the stability of the airstream.

3.2.3. Effect of Different Larynx Widths on the Velocity and Energy Consumption of the Optimized Laval Die. Six optimal parameters of the Laval meltblown die are obtained by the orthogonal test. In order to analyze the relationship influence among the parameters of the orthogonal test, the larynx width of the significant factor was analyzed again by single-factor analysis, keeping the other five parameters unchanged on the basis of the orthogonal test and changing the value of the larynx width. The relationship between larynx width and the maximum airstream velocity and inlet mass flow rate of the optimized meltblown die is obtained, as shown in

Table 5. Range Analysis of the Orthogonal Test

	A	B	C	D	E	F
	b_2 (mm)	b_1/b_2	b_3/b_2	L_2/b_2	L_3/b_2	L_1/b_1
K_1	1501.208	1516.021	1522.444	1514.827	1516.121	1516.700
K_2	1506.320	1517.403	1518.177	1515.657	1512.557	1515.889
K_3	1517.602	1513.851	1515.038	1512.908	1516.028	1512.748
K_4	1523.054	1511.041	1511.199	1515.578	1510.728	1512.267
K_5	1522.622	1512.490	1503.948	1511.836	1515.372	1513.202
k_1	300.242	303.204	304.489	302.965	303.224	303.340
k_2	301.264	303.481	303.635	303.131	302.511	303.178
k_3	303.520	302.770	303.008	302.582	303.206	302.550
k_4	304.611	302.208	302.240	303.116	302.146	302.453
k_5	304.524	302.498	300.790	302.367	303.074	302.640
R_j	4.369	1.272	3.699	0.764	1.079	0.887
effect order of factors	A > C > B > E > F > D					
optimized results	A4B2C1D2E1F1					

Figure 11. When the larynx width increases by 0.2 mm, the increment of the mass flow rate of the meltblown die is
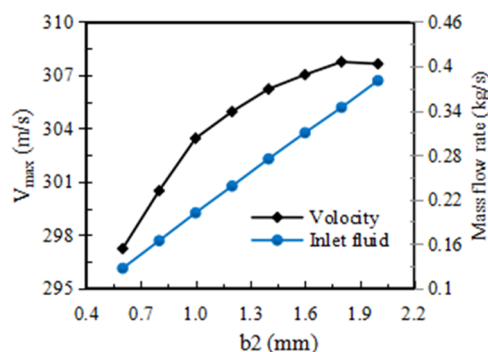
Figure 11. Influence curve of larynx width on the maximum airstream velocity and mass flow rate of Laval die.

basically the same, about 0.036 kg/s, while the increment of the maximum airstream velocity of the meltblown die decreases gradually. From the curve in the figure, it can be seen that when the larynx width increases from 0.6 to 2.0 mm, the increase of the maximum airstream velocity of the meltblown die is 3.261 2.949, 1.505, 1.27, 0.808, 0.719, and −0.113 mm in turn. When the larynx width is 1.8 mm, the peak airstream velocity of the Laval die is the highest, which proves the validity of the orthogonal test results. Therefore, it can be obtained that under the same energy consumption, with the increase in the larynx width, the increase in the maximum air velocity of the meltblown die will continue to decrease until there is an inflection point. In industrial application, in order to reduce energy consumption, in addition to selecting the value of the inflection point, we can consider the loss of part of the velocity and select a smaller throat width, which can greatly reduce the production cost.

3.3. Comparison of the Performance of the Optimized Laval Meltblown Die with that of the Traditional Meltblown Die. This section discusses variations in airspeed, static temperature, airstream pressure, and turbulence intensity along the spinning centerline beneath the meltblown die. Bansal and Shambaugh[40] reported that the average velocity and peak velocity on the centerline below the die directly affect the refinement of the meltblown fiber and that, for traditional meltblown die, most tensile refinement of the fiber occurs in the main stretching zone (i.e., within 15 mm of the meltblown die). Traditional meltblown dies have difficulty maintaining the

stretching velocity of the fiber, and a greater airstream velocity corresponds to a short refinement distance. However, the optimized meltblown die can refine the fiber over a relatively long distance because the airstream velocity and temperature of the optimized die are maintained for a longer time, and the airstream velocity and temperature are maintained at high values. Therefore, the length of the main stretching zone of the optimized Laval meltblown die should exceed 15 mm; therefore, we select a stretching zone extending 40 mm below the spinneret. The performance (airstream velocity, airstream temperature, turbulence intensity, and airstream pressure) of the optimized Laval meltblown die is then analyzed and compared with that of the traditional meltblown die. The structure of the blunt die shown in Figure 1 keeps the other sizes unchanged so that the spinneret width of the traditional die is equal to the spinneret width (0.5 mm) of the Laval die, and the resulting traditional meltblown die is recorded as die 1, which is called a sharp die. In order to compare and analyze the performance of the optimized Laval meltblown die, the air slot width of the traditional die is set to 1.8 mm on the basis of die 1, which is marked as die 2.

3.3.1. Velocity Distribution on the Spinning Centerline of the Meltblown Die. Figure 12 shows the velocity distribution curve along the spinning centerline of a traditional meltblown die and the optimized Laval meltblown die. The airstream velocity curves along the spinning centerline of four meltblown dies all follow the same tendency. Figure 12a shows that as the airstream moves away from the spinneret of the meltblown die, the airstream velocity increases rapidly, is maintained at a higher velocity, continues to increase slightly over a long distance, reaches the maximum velocity (peak velocity), and then decreases continuously. All along the spinning centerline, Laval die 2 has the highest airstream velocity. In the area (<23 mm) near the die spinneret of the meltblown die, the airstream velocities of Laval dies 1 and 2 are greater than those of traditional dies. In a subsequent zone (>23 mm), the airstream velocity of Laval die 1 is slightly lower than that of die 2. Compared with the others, the airstream speed of the optimized Laval die 2 is greatly improved. Along the entire spinning centerline, the average airstream velocities of dies 1 and 2 are 98.81 and 162.32 m/s, and the average airstream velocity of Laval dies 1 and 2 are 156.71 and 194.47 m/s. Compared with the two traditional dies, the average airstream velocity of Laval die 2 increases by 96.81 and 19.81%. Therefore, for the Laval meltblown die optimized by the orthogonal test, the average airstream velocity increases significantly.

(a)

(b)
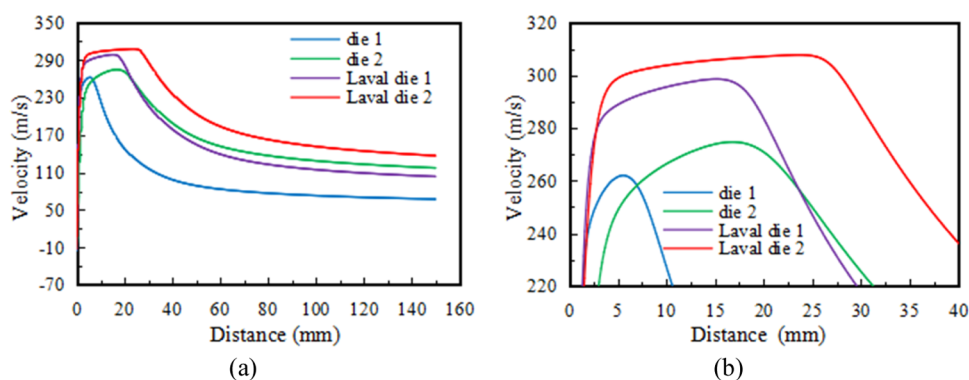
Figure 12. Airstream velocity distribution curves of different meltblown dies: (a) global and (b) local.
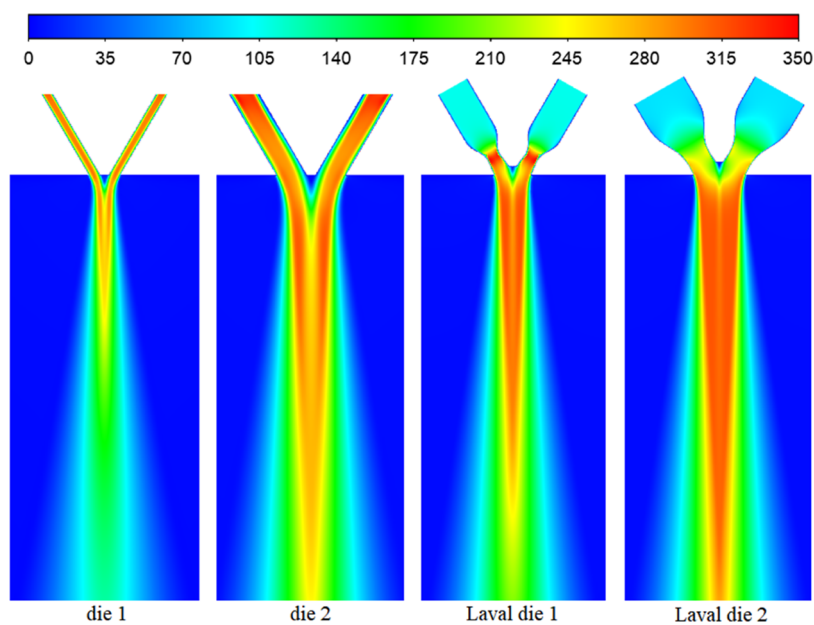
Figure 13. Velocity contours of different meltblown dies.
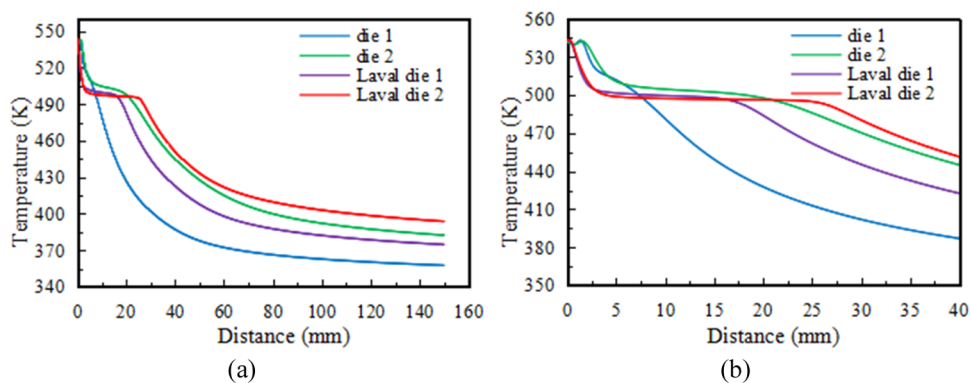
Figure 14. Airstream temperature distribution curves of different meltblown dies: (a) global and (b) local.
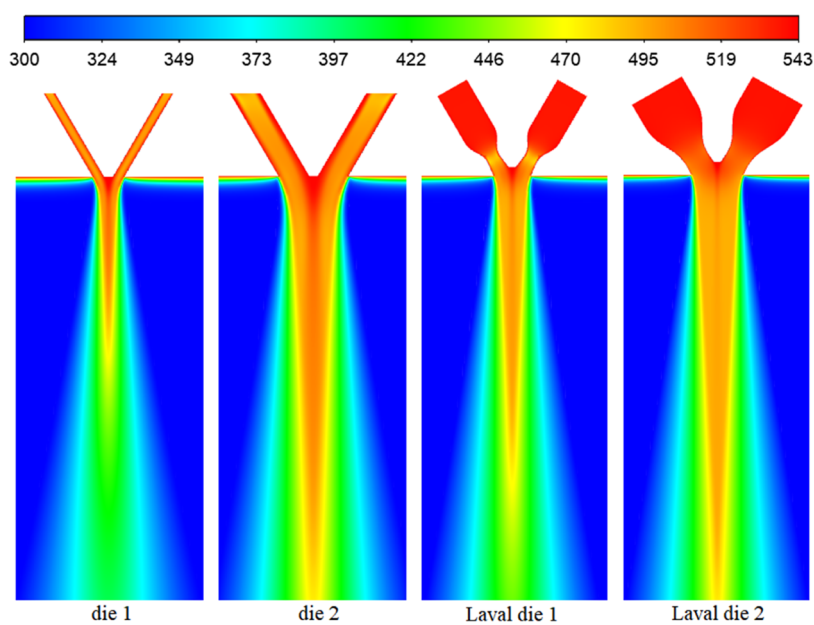
Figure 15. Temperature contours of different meltblown dies.
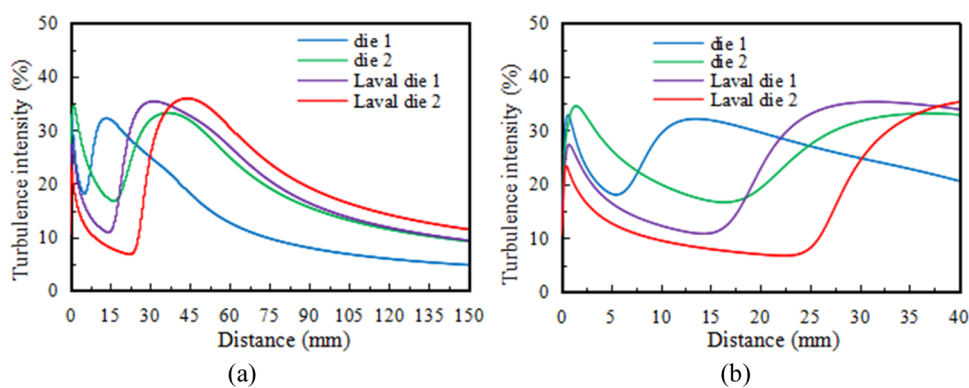
Figure 16. Turbulence intensity distribution curves of different meltblown dies: (a) global and (b) local.

Figure 12b shows the velocity distribution curves in the stretching zone 40 mm from the spinneret on the spinning centerline of the dies. In the stretching zone (0−40 mm), the average airstream velocity for die 1 is 160.88 m/s and the average airstream velocity for Laval die 2 is 283.12 m/s, which is a 75.98% increase with respect to die 1. Therefore, the average airstream velocity in the main stretching zone of the Laval meltblown die optimized by orthogonal testing clearly increases. The peak velocity for die 1 is 262.01 m/s, whereas the peak velocity for Laval die 2 is 307.96 m/s. The peak velocity for Laval die 2 is the largest of the meltblown dies investigated herein and is an increase of 17.54% with respect to the traditional die.

Figure 13 shows the airstream velocity contours of the different meltblown dies. The airstream velocity has a direct effect on the tensile refinement of the meltblown fibers. Laval die 2 has the largest peak airstream velocity, which is maintained over a long distance. The airstream velocity characteristic of Laval die 2 is very advantageous for refining polymer fibers. Laval die 2 has a clear advantage due to its airstream velocity, which accelerates the attenuation of the fiber diameter and helps produce more fine nanofibers. Therefore, changing the airstream channel of the meltblown die from the parallel structure of the traditional die to the Laval structure clearly improves the airstream velocity and peak velocity of the meltblown die, with a concomitant improvement in the overall performance.

3.3.2. Temperature Distribution on the Spinning Centerline of the Meltblown Die. Figure 14 shows the temperature distribution along the spinning centerline for the traditional meltblown die and the optimized meltblown die, and the airstream temperature curves on the spinning centerline for the four meltblown dies. The curves all follow a similar tendency: the only difference being that, farther from the spinneret, the airstream temperature of the traditional die decreases continuously, whereas that of the Laval dies remains essentially constant after 3 mm. In particular, the temperature of Laval die 2 remains constant over the longest distance (3−25 mm), as seen in detail in Figure 15. Over the range of 0−7 mm on the spinning centerline, the airstream temperature of Laval die 2 is slightly lower than that of die 1, and the airstream temperature of Laval die 2 is much higher than that of die 1 in the rest range (>7 mm); in the range of 0−17 mm, the airstream temperatures of two Laval dies are basically the same, and the airstream temperature of Laval die 2 is much higher than that of Laval die 1 in the rest range (>17 mm); in the range of 0−22 mm, the airstream temperature of Laval die 2 is slightly

lower than that of die 2, and the airstream temperature of Laval die 2 is higher than that of die 2 in the rest range (>22 mm). In the main stretching zone (from 0 to 40 mm from the spinneret), the average temperature for die 1 is the lowest (442.98 K), and the average temperature for Laval die 2 is the highest (489.87 K), an increase of 10.59% with respect to that of the traditional die. Thus, Laval die 2 optimized by the orthogonal test produces the highest, most stable temperature in the airstream.

Although a greater airstream temperature can soften the polymer and enhance its fluidity, it has no immediate impact on the refinement of the meltblown fiber. According to the analysis of Figures 14b and 12b, the peak velocity of Laval die 2 occurs at 22 mm below the spinneret, where the airstream temperature is also higher than that of the other three dies, allowing better refinement of the polymer. Given the higher airstream temperature and velocity in the main stretching zone of Laval die 2, the polymer fiber is easier to stretch and refine and more nanofibers are produced.

3.3.3. Turbulence Intensity Distribution along the Spinning Centerline of the Meltblown Die. Figure 16 shows the turbulence intensity distribution along the centerline of the traditional meltblown die and the Laval meltblown die. The results for the four meltblown dies all follow a similar tendency. Near the spinneret, the turbulence intensity peaks for all four dies. The peak turbulence intensity of the Laval meltblown dies is lower than that of the traditional meltblown dies, indicating that the airstream from the Laval nozzle is relatively stable and the airstream is relatively stable. Laval die 2 has the lowest peak turbulence intensity. In the range of 0−30 mm on the spinning centerline, the turbulence intensity for Laval die 2 is lower than that of the other dies; in the range of 0−36 mm, the turbulence intensity of Laval die 2 is lower than that of die 2; in the range of 0−38 mm, the turbulence intensity of Laval die 2 is lower than that of Laval die 1; in the region greater than 38 mm, the turbulence intensity of Laval die 2 is the highest. Turbulence intensity is an important index of the stability of the airstream. Generally speaking, if the airstream has a larger turbulence intensity, the fiber will whip to a certain extent with the disturbance of the airstream, which is beneficial to the stretching of the fiber; if the turbulence intensity of the airstream is smaller, it indicates that the softer the meltblown flow, the smoother the fiber.

However, in the region near the spinneret hole, Laval die 2 with a small turbulence intensity is beneficial to the fiber-stretching process because the smaller turbulence intensity near the spinneret hole makes the airstream more stable, which

can effectively reduce the effect of airstream disorder on the fiber-stretching process, effectively reduce the adhesion and fracture between the melted fibers, and effectively prevent the polymer melt from blocking the spinneret of the die. In the nonmain stretching zone far from the spinneret, because the fiber has solidified or tends to solidify, a larger turbulence intensity will not only cause adhesion and fracture to the fiber but also is conducive to the extension and refinement of the fiber. Therefore, Laval die 2 has a smaller turbulence intensity near the spinneret hole and a larger turbulence intensity away from the spinneret hole, which makes it more advantageous than a traditional die.

3.3.4. Air Pressure Distribution on the Spinning Centerline of the Meltblown Die. Figure 17 shows the air pressure
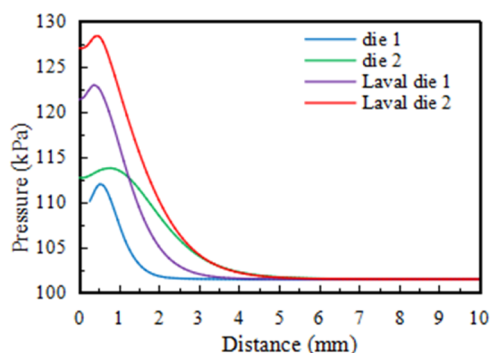
Figure 17. Air pressure distribution curves of different meltblown dies.

distribution along the spinning centerline of the traditional die and the Laval meltblown dies. The curves along the spinning centerline of all meltblown dies follow a similar tendency. The airstream pressure peaks near the spinneret: the peak pressure of the traditional die is the smallest, and the Laval meltblown die produces a larger peak pressure. Laval die 2 produces the highest pressure along the spinning centerline at 0−5.5 mm from the spinneret. Beyond 5.5 mm, the pressure produced by the four meltblown dies almost equals the atmospheric pressure.

The pressure characteristic of the airstream is a significant factor affecting the polymer stretching. A greater airstream pressure acts directly on the face of the meltblown fibers, thus affecting the shape and area of the fiber cross section and the

fiber refinement. The change in the cross-sectional shape directly affects the friction between the airstream and the polymer fiber, possibly increasing the force exerted on the fiber. This effect helps to produce thinner fibers.[41] The peak pressure of Laval die 2 is 128.3 kPa, the peak pressure of die 1 is 111.94 kPa, and the peak pressure of Laval die 2 is 14.61% higher than that of die 1. Laval die 2 produces a large pressure difference with the airstream, and the forced extrusion of the airstream on the polymer fibers at a high velocity and high temperature helps to extend and thin the polymer fibers, thereby producing more nanofibers.

3.4. Effect of Inlet Pressure on the Airstream Velocity of the Meltblown Die. We know that a Laval nozzle can accelerate low-speed airstream into high-speed airstream and even accelerate airstream from subsonic to supersonic. The maximum airstream velocity obtained from the previous analysis of the Laval meltblown die does not reach the supersonic effect, which is due to the fact that the inlet pressure of the meltblown die is too small. In order to achieve supersonic velocity on the spinning centerline of the optimized Laval die, the effect of inlet pressure on the airstream velocity of the Laval meltblown die was studied. The inlet pressure of the optimized Laval die is set to seven groups (1.4 1.6, 1.8, 2.0, 2.2, 2.4, and 2.6 atm). The variation curves of the airstream velocity of the Laval meltblown die under different inlet pressures are shown in Figure 18.

It can be seen from Figure 18 that the airstream velocity curves on the spinning centerline of the meltblown die show a similar trend under different inlet pressures, and the distance maintained by the larger airstream velocity increases with the increase of inlet pressure. When the inlet pressure increases by 0.2 atm, the increase of the airstream velocity becomes smaller; when the inlet pressure is greater than 1.6 atm, the supersonic airstream can be obtained; when the inlet pressure is less than 2.0 atm, at any position on the spinning centerline, the airstream velocity increases with the increase of inlet pressure; and when the inlet pressure is greater than 2.0 atm, the airstream velocity of the die generally increases with the increase of the inlet pressure. However, near the spinneret of the die, the meltblown airstream will oscillate, the airstream velocity will fluctuate, and a pulsating airstream will appear, which is called the shock wave. It is worth noting that the greater the inlet pressure, the more the number of shock waves, and the larger the wavelength of the shock wave, the greater the amplitude of the shock wave. The closer the spinneret, the
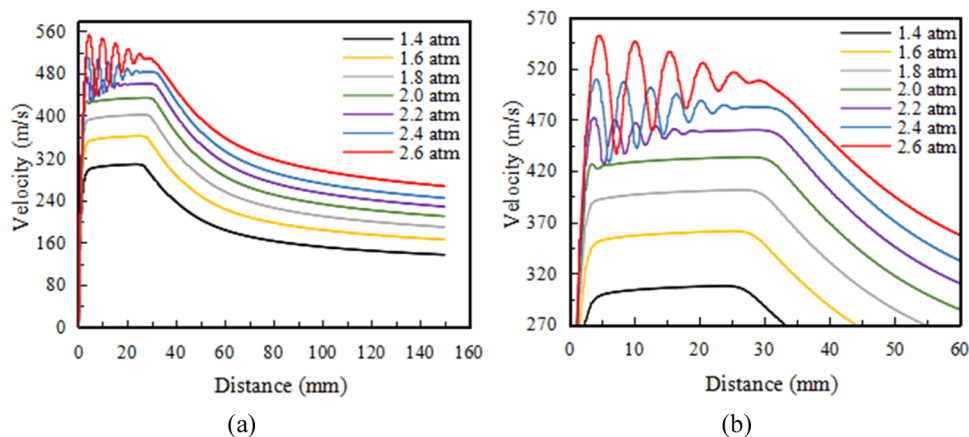
Figure 18. Airstream velocity curve of meltblown die under different inlet pressures: (a) global and (b) local.

larger the amplitude of the shock wave, and vice versa, until the shock wave disappears. According to the research of Tyagi and Shambaugh,[42] if the airstream velocity fluctuates in the main stretching zone, the pulsating airstream can effectively promote the stretching of the polymer and reduce the fiber diameter, which is beneficial to fiber refinement.

4. CONCLUSIONS

This article analyzes and improves the airstream channel of a meltblown die. We propose a new type of meltblown die with a Laval airstream channel structure. We design a two-dimensional model of a Laval meltblown die and simulate the airstream field of a traditional meltblown die and various Laval meltblown dies by using the SST k-ω turbulence model in CFD. The six main factors that determine the structure of the Laval airstream channel are analyzed, and the optimum configuration is obtained by single-factor analysis. Given that the performance of the Laval meltblown die depends on several interrelated factors, the Laval channel structure was further analyzed by using a six-factor, five-level orthogonal test. Based on this test, we discuss how multiple factors affect the airstream peak velocity along the spinning line beneath the meltblown die and obtain optimal parametrization. The parametrization obtained by single-factor analysis results in a Laval meltblown die that performs less well than the same dye parametrized by the multifactor orthogonal test. Finally, the optimized Laval meltblown die and the traditional meltblown die were compared and analyzed, producing the following conclusions.

(1) The maximum velocity along the spinning line beneath the meltblown die grows with the growth of the larynx width, but the bigger the larynx width, the more energy consumption in the fiber production process; the entrance width of the shrinkage segment is not the larger the better, the critical value b_1/b_2 is 2.4; b_3/b_2 should be as small as possible, and the value of b_3/b_2 is 1.05; to ensure uniform airstream and greater acceleration capacity, the length of the contraction segment should be moderate, and the value of L_2/b_2 should be 2.1; with the growth of L_3/b_2, it can be approximately considered that the airstream peak velocity grows at first and then decreases, and the value of L_3/b_2 is 1.0; to stabilize the airstream and reduce the loss along the way, the length of the stable segment should be moderate, and the value of L_1/b_1 is 1.0.

(2) An orthogonal test was used to analyze the six factors that define the Laval structure. The results show that the factors b_3/b_2 and b_2 most strongly influence the airstream velocity beneath the Laval meltblown die. The optimal parametrization of the Laval airstream channel is as follows: the larynx width is 1.8 mm, the inlet width of the contraction segment is 4.14 mm, the outlet width of the expansion segment is 1.89 mm, the length of the contraction segment is 3.78 mm, the length of the expansion segment is 0.72 mm, and the length of the stable segment is 2.07 mm. The Laval meltblown die with this parametrization performs optimally.

(3) The meltblown die with the Laval airstream channel has a greatly increased average airstream velocity and peak airstream velocity along the spinning centerline. With respect to the traditional meltblown die, the peak airstream velocity of Laval die 2 optimized by orthogonal testing increases by 17.54%, the average air velocity in the 0−40 mm stretching zone increases by 75.98%, and the average temperature in the same zone increases by 12.32%. Higher airstream temperature and higher airstream velocity more effectively refine the polymer, thereby accelerating the attenuation of the fiber diameter and producing more and finer nanofibers.

(4) Compared with the traditional meltblown die, the Laval die 2 optimized by orthogonal testing produces a lower turbulence intensity and a more stable and uniform airstream near the spinneret, which decrease the influence of airstream disorder on fiber-stretching. Laval die 2 also produces the largest peak pressure of all dies studied herein. The forced extrusion of the high-velocity and high-temperature airstream on the polymer fiber helps to thin the meltblown fiber.

This paper provides a specific and effective method to design and optimize a meltblown die, providing a technical reference for meltblown production equipment for the actual production and application of meltblown fibers. It also lays a technical foundation for follow-up studies of the performance of other types of meltblown dies.

■ AUTHOR INFORMATION

Corresponding Author
Zhisong Zhu − *School of Mechanical Engineering, Nantong University, Nantong 226019, China*; Email: zhu.zhs@ntu.edu.cn

Author
Dongjun Guo − *Engineering Training Center, Nantong University, Nantong 226019, China*; ● orcid.org/0000-0001-7316-5525

Complete contact information is available at:
https://pubs.acs.org/10.1021/acsomega.3c05643

Notes
The authors declare no competing financial interest.

■ REFERENCES

(1) Han, W.; Bhat, G. S.; Wang, X. Investigation of nanofiber breakup in the melt-blowing process. *Ind. Eng. Chem. Res.* **2016**, *55*, 3150−3156.

(2) Hassan, M. A.; Yeom, B.; Wilkie, A.; Pourdeyhimi, B.; Khan, S. A. Fabrication of nanofiber meltblown membranes and their filtration properties. *J. Membr. Sci.* **2013**, *427*, 336−344.

(3) Burger, C.; Hsiao, B. S.; Chu, B. Nanofibrous materials and their applications. *Annu. Rev. Mater. Res.* **2006**, *36*, 333−368.

(4) Wang, Z.; Macosko, C. W.; Bates, F. S. Fluorine-enriched melt-blown fibers from polymer blends of poly(butylene terephthalate) and a fluorinated multiblock copolyester. *ACS Appl. Mater. Interfaces* **2016**, *8*, 3006−3012.

(5) Drabek, J.; Zatloukal, M. Influence of molecular weight, temperature, and extensional rheology on melt blowing process stability for linear isotactic polypropylene. *Phys. Fluids* **2020**, *32*, No. 083110.

(6) Ji, C.; Wang, Y.; Sun, Y. Numerical investigation on a melt-blowing die with internal stabilizers. *J. Ind. Text.* **2021**, *50*, 1409−1421.

(7) Han, W.; Xie, S.; Shi, J.; Wang, X. Study on airstream field and fiber motion with new melt blowing die. *Polym. Eng. Sci.* **2019**, *59*, 1182−1189.

(8) Xin, S.; Wang, X. Investigation into the effect of the angle of dual slots on an airstream field in melt blowing via numerical simulation. *e-Polymers* **2016**, *16*, 337−342.

(9) Sun, Y.; Zeng, Y.; Wang, X. Three-dimensional model of whipping motion in the processing of microfibers. *Ind. Eng. Chem. Res.* **2011**, *50*, 1099−1109.

(10) Harpham, A. S.; Shambaugh, R. L. Flow field of practical dual rectangular jets. *Ind. Eng. Chem. Res.* **1996**, *35*, 3776−3781.

(11) Harpham, A. S.; Shambaugh, R. L. Velocity and temperature fields of dual rectangular jets. *Ind. Eng. Chem. Res.* **1997**, *36*, 3937−3943.

(12) Bresee, R. R.; Ko, W. C. Fiber formation during melt blowing. *Int. Nonwovens J.* **2003**, *os-12*, 21−28.

(13) Xie, S.; Zeng, Y. Turbulent airstream field and fiber whipping motion in the melt blowing process: experimental study. *Ind. Eng. Chem. Res.* **2012**, *51*, 5346−5352.

(14) Xie, S.; Han, W.; Jiang, G.; Chen, C. Turbulent airstream field in slot-die melt blowing for manufacturing microfibrous nonwoven materials. *J. Mater. Sci.* **2018**, *53*, 6991−7003.

(15) Yang, Y.; Zeng, Y. Simultaneous measurement in non-isothermal melt-blowing airstream field: time-averaged and turbulent characteristics. *Ind. Eng. Chem. Res.* **2020**, *59*, 10664−10672.

(16) Yang, Y.; Zeng, Y. Measurement and Comparison of Melt-Blowing airstream Fields: Nozzle Modifications to Reduce Turbulence and Fibre Whipping. *Polymers* **2021**, *13*, No. 719, DOI: 10.3390/polym13050719.

(17) Hassan, M. A.; Anantharamaiah, N.; Khan, S. A.; Pourdeyhimi, B. Computational fluid dynamics simulations and experiments of meltblown fibrous media: new die designs to enhance fiber attenuation and filtration quality. *Ind. Eng. Chem. Res.* **2016**, *55*, 2049−2058.

(18) Shambaugh, R. L.; Krutty, J. D.; Singleton, S. M. Melt Blowing Dies with Louvers. *Ind. Eng. Chem. Res.* **2015**, *54*, 12999−13004.

(19) Zhao, B. Numerical simulation the air jet flow field of a dual slot inset blunt die in the melt blowing nonwoven process. *Polym. Eng. Sci.* **2018**, *58*, 1817−1825.

(20) Tate, B. D.; Sambaugh, R. L. Modified dual rectangular jets for fiber production. *Ind. Eng. Chem. Res.* **1998**, *37*, 3772−3779.

(21) Krutka, H. M.; Shambaugh, R. L.; Papavassiliou, D. V. Analysis of a melt-blowing die: Comparison of CFD and experiments. *Ind. Eng. Chem. Res.* **2002**, *41*, 5125−5138.

(22) Krutka, H. M.; Shambaugh, R. L.; Papavassiliou, D. V. Analysis of multiple jets in the schwarz melt-blowing die using computational fluid dynamics. *Ind. Eng. Chem. Res.* **2005**, *44*, 8922−8932.

(23) Krutka, H. M.; Shambaugh, R. L.; Papavassiliou, D. V. Analysis of the temperature field from multiple jets in the schwarz melt blowing die using computational fluid dynamics. *Ind. Eng. Chem. Res.* **2006**, *45*, 5098−5109.

(24) Sun, Y.; Wang, X. Optimization of airstream field of the melt blowing slot die via numerical simulation and genetic algorithm. *J. Appl. Polym. Sci.* **2010**, *115*, 1540−1545.

(25) Sun, Y.; Wang, X. Optimal geometry design of the melt-blowing slot die with high stagnation temperature via the orthogonal array method and numerical simulation. *J. Text. Inst.* **2011**, *102*, 65−69.

(26) Xie, S.; Jiang, G.; Wu, X.; Wang, Y.; Fang, H.; Shentu, B. Q. Air recirculation and its effect on microfiber spinning in blunt-die melt blowing. *Fibers Polym.* **2021**, *22*, 703−710.

(27) Hao, X.; Huang, H.; Zeng, Y. Simulation of jet velocity in the melt-blowing process using the coupled air polymer model. *Text. Res. J.* **2019**, *89*, 3221−3233.

(28) Yang, Y.; Huang, H.; Zeng, Y. C. Turbulence of melt-blowing airstream field: Comparison of a convergent jet and a typical free jet. *Phys. Fluids* **2021**, *33*, No. 075107.

(29) Wang, Y.; Zhou, J.; Gao, X. Numerical analysis of airstream fields from new melt-blowing dies for dual-slot jets. *ACS Omega* **2020**, *5*, 13409−13415.

(30) Xu, H.; Zhou, Z.; Liu, J.; Zhao, L.; Xie, S.; Zhang, J. Preliminary study of the effect of secondary airstream on fiber attenuation during melt blowing. *Fibers Polym.* **2022**, *23*, 3039−3045.

(31) Hao, X.; Jiang, G.; Tao, J.; Liu, G.; Xie, S. Experimental and Simulation Investigation on the Effect of Slot Angle on the Flush Sharp Die Performance during Melt Blowing. *Fibers Polym.* **2022**, *23*, 2725−2731.

(32) Durif, O. Design of de Laval nozzles for gas-phase molecular studies in uniform supersonic flow. *Phys. Fluids* **2022**, *34*, No. 013605.

(33) Rong, G.; Cheng, M.; Sheng, Z.; Liu, X.; Zhang, Y.; Wang, J. Investigation of counter-rotating shock wave and wave direction control of hollow rotating detonation engine with Laval nozzle. *Phys. Fluids* **2022**, *34*, No. 056104.

(34) Tan, D. H.; Herman, P. K.; Janakiraman, A.; Bates, F. S.; Kumar, S.; Macosko, C. W. Influence of Laval nozzles on the airstream field in melt blowing apparatus. *Chem. Eng. Sci.* **2012**, *80*, 342−348.

(35) Menter, F. R. Two-equation eddy-viscosity turbulence models for engineering applications. *AIAA J.* **1994**, *32*, 1598−1605.

(36) Tepe, A. U. Numerical investigation of a novel jet hole design for staggered array jet impingement cooling on a semicircular concave surface. *Int. J. Therm. Sci.* **2021**, *162*, No. 106792.

(37) Abadi, S. M. H. B.; Zirak, S.; Zargarabadic, M. R. Effect of pulsating injection and mainstream attack angle on film cooling performance of a gas turbine blade. *Phys. Fluids* **2020**, *32*, No. 117102.

(38) Jin, W.; Jia, Y.; Lei, J.; Ji, W.; Wu, J. Coupled heat transfer analysis of internal and film cooling of turbine blade under medium temperature conditions. *Appl. Therm. Eng.* **2022**, *214*, No. 119192.

(39) Wang, R.; Xiao, Z. Transition effects on flow characteristics around a static two-dimensional airfoil. *Phys. Fluids* **2020**, *32*, No. 035113.

(40) Bansal, V.; Shambaugh, R. L. On-line determination of diameter and temperature during melt blowing of polypropylene. *Ind. Eng. Chem. Res.* **1998**, *37*, 1799−1806.

(41) Guo, D.; Fan, H.; Zhu, Z.; Xiao, K. Numerical investigation into the effect of geometric shape of slot on airstream field in meltblown for polymer fiber. *J. Text. Inst.* **2022**, *113*, 1133−1141.

(42) Tyagi, M. K.; Shambaugh, R. L. Use of oscillating gas jets in fiber processing. *Ind. Eng. Chem. Res.* **1995**, *34*, 656−660.